WELL-BALANCED FINITE VOLUME SCHEMES OF ARBITRARY ORDER OF ACCURACY FOR SHALLOW WATER FLOWS

SEBASTIAN NOELLE, NORMANN PANKRATZ, GABRIELLA PUPPO, AND JOSTEIN R. NATVIG

Abstract. Many geophysical flows are merely perturbations of some fundamental equilibrium state. If a numerical scheme shall capture such flows efficiently, it should be able to preserve the unperturbed equilibrium state at the discrete level. Here we present a class of schemes of any desired order of accuracy which preserve the lake at rest perfectly. These schemes should have an impact for studying important classes of lake and ocean flows.

Contents

Date: Submitted to JCP on March 18, 2005.

Key words and phrases. hyperbolic conservation laws, source terms, shallow water equations, well-balanced schemes, finite volume schemes, WENO reconstruction.

This joint work was supported by the EU financed network no. HPRN-CT-2002-00282 ("Hyke"). The work of N.P. was funded by German Science Foundation grant Graduiertenkolleg 775 and that of J.N. by the BeMatA program of the Norwegian Research Council.

1. Introduction

In this introduction, we present some of the key ideas and ingredients of the subsequent sections. We begin with a brief review of the shallow water equations and their equilibrium states, in particular the lake at rest. Then we show an example of a numerical storm produced by a scheme which is not in discrete equilibrium. Next we review the key ingredient of several of the recent well-balanced schemes, and give some related references. We close with a preview of our new high order well-balanced schemes.

1.1. **Shallow Water Equations.** Many geophysical flows are modeled by variants of the shallow water equations. In their simplest form these equations read

$$\begin{aligned} h_t + (hu)_x &= 0, \\ (hu)_t + (hu^2 + \tfrac{1}{2}gh^2)_x &= -ghz_x. \end{aligned} \tag{1}$$

Here $z(x)$ defines the bottom-topography, $h(x,t)$ denotes the water height above the bottom, and $u(x,t)$ is the horizontal component of the water velocity at position x at time t. The gravity constant is denoted by g. In (1) we have neglected two-dimensional effects, bottom friction, Coriolis forces arising in a rotational frame, wind forces, and, of course, vertical variations of the velocity field. For an example of more complete shallow water equations which are used in coastal engineering, we refer to Gjevik et al. [10].

1.2. **Equilibrium States.** In spite of all of these simplifications, the equations (1) still contain the most fundamental balances of shallow water flows. The convective part on the left-hand-side (LHS) is a hyperbolic system of conservation laws similar to that of compressible fluid flows, and the source term on the right-hand-side (RHS) is due to gravitational acceleration. Let us look at the equilibrium, or stationary, states. They are given by

$$hu \equiv \text{const} \quad \text{and} \quad \frac{1}{2}u^2 + gH \equiv \text{const},$$

where

$$H := h + z$$

is the water level. In this paper we are particularly interested in the lake at rest, given by

$$u \equiv 0 \quad \text{and} \quad H \equiv \text{const}.$$

Such a situation is shown in Figure 1 for a cross-section of lake Rursee near Aachen. Let us pause for a moment and look at this balance once more. From (1) and the assumptions of stationary flow with vanishing velocity we have

$$0 = \left(g\frac{h^2}{2}\right)_x + ghz_x, \tag{2}$$

which is called hydrostatic balance. The first term is the hydrostatic pressure, which models the tendency of a column of water to collapse vertically and at the same time expand laterally under the influence of gravity. The second term is the gravitational acceleration down an inclined bottom z. Now use the chain rule of differentiation and divide by h to obtain

$$0 = g\,(h+z)_x = gH_x.$$

Thus we see that the effective acceleration can be interpreted as gravitational acceleration down a non-flat water level H.

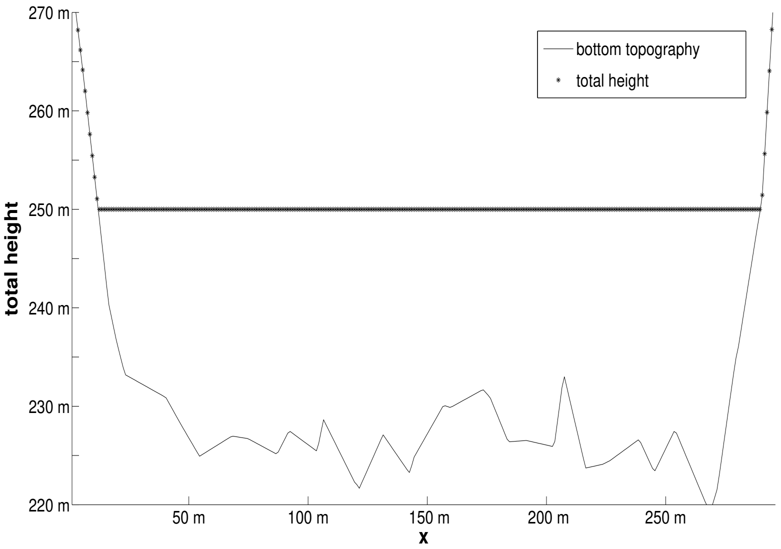

FIGURE 1. Cross section of lake Rursee: bottom topography and quiet water level. 296 cells

1.3. **Numerical Storms.** If a numerical scheme does not preserve the fundamental balance (2) at the discrete level, this may result in spurious oscillations, or numerical storms, as seen in Figure 2. The figure shows a cross-section of lake Rursee near Aachen, and the water should remain at rest as in Figure 1. Thus, all waves in Figure 2 are pure numerical artifacts. Some of them are more than a meter high, especially near the edge of the lake. The computation is run with a standard finite volume scheme, a naive treatment of the source term, and 296 spatial grid cells. Clearly, this scheme on the current grid would not be able to resolve waves which are of the order of magnitude of the numerical perturbations. One would therefore have to run such a scheme with a much finer grid, which would make the computation rather costly.

1.4. **Well-Balanced Schemes.** The results in Figure 3, which reproduce the lake at rest perfectly, are obtained with a so-called well-balanced scheme, using the same number of spatial grid cells and timesteps. Let us briefly sketch the main ingredient of the discrete balance which makes the scheme successful. The main difficulty for the schemes is to preserve the balance of hydrostatic pressure and gravitational acceleration (hydrostatic balance). Given a cell $[x_L, x_R]$, let $h_L = h(x_L), h_R = h(x_R)$. A conservative finite volume discretization of the hydrostatic pressure would then be

$$\begin{aligned} \left(g\,\frac{h^2}{2}\right)_x &\approx g\,\frac{h_R^2 - h_L^2}{2\Delta x} \\ &= g\,\frac{h_L + h_R}{2}\,\frac{h_R - h_L}{\Delta x}. \end{aligned}$$

We will now show that this already implies a canonical well-balanced discretization of the source term. Indeed, suppose that the source term is discretized as

$$ghz_x \approx g\bar{h}Dz,$$

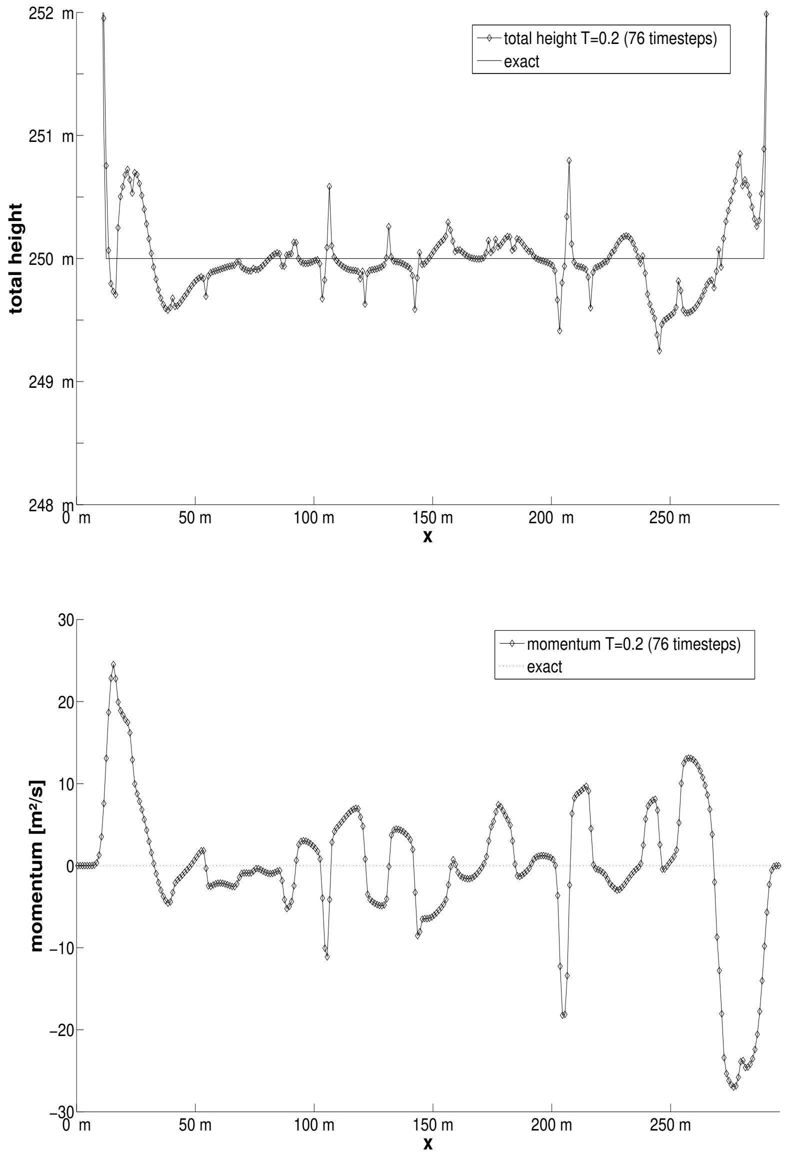

FIGURE 2. Numerical storm over lake Rursee, produced by a naive finite volume scheme: water level (top) and momentum (bottom) at time $T = 0.2$ (76 time steps)

where $\bar{h} \approx h$ and $Dz \approx z_x$. Now we suppose that $u \equiv 0$ and $H \equiv \text{const}$, and we want to enforce the discrete hydrostatic balance

$$0 = g\frac{h_L + h_R}{2}\frac{h_R - h_L}{\Delta x} + g\bar{h}Dz. \tag{3}$$

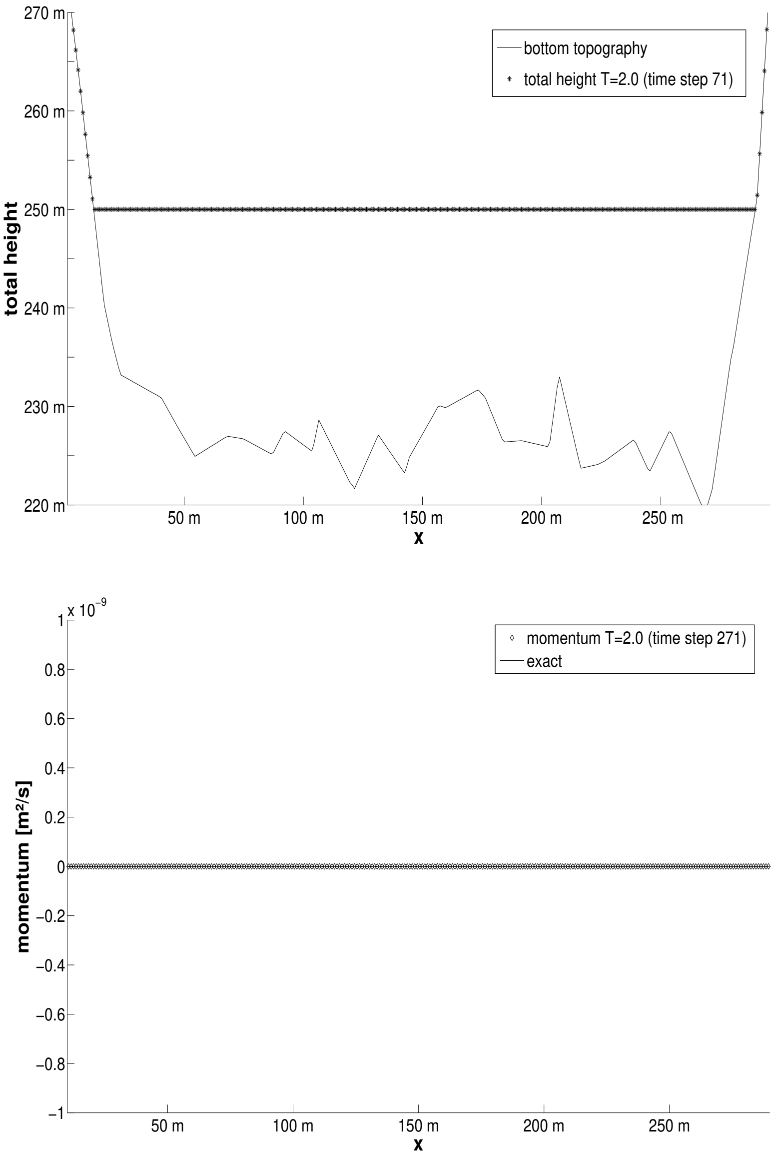

FIGURE 3. Well-balanced computation of quiet lake Rursee: water level (top) and momentum (bottom) at time $T = 0.2$ (71 time steps). Note that the scale of the momentum axis is 10^{-9}.

From (3) we obtain

$$\begin{aligned} \bar{h}Dz &= -\frac{h_L + h_R}{2}\frac{h_R - h_L}{\Delta x} \\ &= -\frac{h_L + h_R}{2}\frac{(H_R - z_R) - (H_L - z_L)}{\Delta x} \\ &= \frac{h_L + h_R}{2}\frac{z_R - z_L}{\Delta x}. \end{aligned} \tag{4}$$

This discretization of the source term was first proposed by Bermudez and Vazquez [3], and it is also the essential ingredient of the recent well-balanced schemes of Kurganov and Levy and Audusse et al. [20, 1]. Closely related schemes usually try to discretize the derivative of the convective flux and the source term by one and the same finite difference or finite volume operator, see [2, 4, 30]. Greenberg, LeRoux and coworkers developed schemes based on the solution of the non-homogenous Riemann-problem, see [14, 12, 11]. We would also like to mention the finite volume Roe schemes of Gallouët and coworkers [9] and the Norwegian front tracking approach [15]. This list is by far not exhaustive, and we refer to the papers mentioned above for further references.

Our paper is based on the recent work of Audusse, Bristeau, Bouchut, Klein and Perthame (2004) [1]. Their first and second order schemes preserve positivity of water height and the lake at rest. The first order scheme also satisfies a discrete entropy inequality at discontinuities.

In the present paper we are interested in very high order accurate well-balanced schemes. These more sophisticated schemes are needed if, for instance, one wants to track small waves over long periods of time. Well-balanced *finite difference* schemes of high order of accuracy were developed by Vukovic and Sopta 2002 [29] and Xing and Shu 2004 [30]. Here we extend the well-balanced *finite volume* schemes of Audusse et al. [1] to any desired order of accuracy.

We would like to stress that the approach to achieve high order is rather different in the case of finite difference and finite volume schemes. In the former case, Xing and Shu rewrite the balance law in such a way that the fluxes and source terms can be treated by one and the same difference operator. In the present paper, we observe that the well-balanced quadrature (4) maintains all its desirable properties under numerical extrapolation. Together with standard high order reconstructions and the hydrostatic correction this leads immediately to the desired very high order accurate well-balanced *finite volume* schemes. This technique can be applied to many, if not all, of the second order well-balanced schemes based on (4). Numerical experiments show the expected convergence rates for a fourth/fifth order version of our new scheme, and excellent resolution of discontinuities and very small disturbances.

Acknowledgement: The authors would like to thank Francois Bouchut for lively and stimulating discussions. Francois Bouchut gave us a version of his first and second order well-balanced scheme. We would also like to thank the Institute of Hydraulic Engineering and Water Resources Management of RWTH Aachen for providing the topographical data of lake Rursee.

2. High Order Well-Balanced Schemes

In this section, we first summarize the second order well-balanced scheme of Audusse et al. [1]. Then, for any order of accuracy, we introduce our new treatment of the source term. We close the section with a summary of the new algorithm. Details of the WENO reconstruction are given in Appendix A.

2.1. **Review of Second Order Well-Balancing via Hydrostatic Reconstruction.**

Let $U := (h, hu)^T$ be the vector of conservative variables. First we formulate a semidiscrete finite volume scheme for the cell averages,

$$U_i(t) := \frac{1}{\Delta x_i} \int_{x_{i-\frac{1}{2}}}^{x_{i+\frac{1}{2}}} U(x,t)dx,$$

with $\Delta x_i := x_{i+\frac{1}{2}} - x_{i-\frac{1}{2}}$. Based on these cell averages, one defines a piecewise polynomial reconstruction, which will in general be discontinuous at the interfaces $x_{i+\frac{1}{2}}$. Oscillations will be suppressed with limiters. Audusse et al. use a linear reconstruction with minmod limiter, which leads to a second order scheme. Within cell i, the left and right values of each component at position $x_{i-\frac{1}{2}} + 0$ respectively $x_{i+\frac{1}{2}} - 0$ are denoted by $(.)_{i,l}$ and $(.)_{i,r}$.

Audusse et al. reconstruct h, H, and u. From this, the bottom topography is computed as $z = H - h$. This leaves the lake at rest unperturbed, but it leads to a discontinuous bottom. To get a stable and well-balanced scheme, the following hydrostatic reconstruction is introduced:

$$h^*_{i,r} := \max(0, h_{i,r} + z_{i,r} - \max(z_{i,r}, z_{i+1,l})), \tag{5}$$

$$h^*_{i+1,l} := \max(0, h_{i+1,l} + z_{i+1,l} - \max(z_{i,r}, z_{i+1,l})). \tag{6}$$

These values are used to construct auxiliary values $U^*_{i,r}$ and $U^*_{i+1,l}$ which will enter an approximate Riemann solver:

$$U^*_{i,r} : \begin{pmatrix} h^*_{i,r} \\ h^*_{i,r} u_{i,r} \end{pmatrix}$$

$$U^*_{i+1,l} : \begin{pmatrix} h^*_{i+1,l} \\ h^*_{i+1,l} u_{i+1,l} \end{pmatrix}.$$

Note that at the interface $x_{i+\frac{1}{2}}$, we have two different reconstructions, namely $x_{i+\frac{1}{2}-}$ on the left and $x_{i+\frac{1}{2}+}$ on the right side. The semidiscrete finite volume scheme then reads

$$\Delta x_i \frac{d}{dt} U_i(t) - \mathcal{F}_l(U_i, U_{i+1}, z_{i,r}, z_{i+1,l}) + \mathcal{F}_r(U_{i-1}, U_i, z_{i-1,r}, z_{i,l}) = S^{(j)}_{ci}. \tag{7}$$

It remains to specify the numerical fluxes and the source term. The fluxes are given by

$$\mathcal{F}_r(U_i, U_{i+1}, z_{i,r}, z_{i+1,l}) := F(U^*_{i,r}, U^*_{i+1,l}) + \begin{pmatrix} 0 \\ \frac{g}{2} h^2_{i,r} - \frac{g}{2}(h^*_{i,r})^2 \end{pmatrix} \tag{8}$$

$$\mathcal{F}_l(U_{i-1}, U_i, z_{i-1,l}, z_{i,r}) := F(U^*_{i-1,r}, U^*_{i,l}) + \begin{pmatrix} 0 \\ \frac{g}{2} h^2_{i,l} - \frac{g}{2}(h^*_{i,l})^2 \end{pmatrix} \tag{9}$$

Here F is a conservative numerical flux consistent with the homogeneous shallow water equations. Because of their robustness, the local Lax-Friedrichs, Harten-Lax-vanLeer or kinetic solvers are used in [1] and also in the present paper. The second term on the RHS of (8) and (9) cancels the difference of the hydrostatic pressures based on the piecewise polynomial reconstruction $h_{i,r}$ and the hydrostatic reconstruction $h^*_{i,r}$ at the interface $x_{i+\frac{1}{2}}$.

The index $j = 1, 2$ represents the order of the numerical source term $S^{(j)}_{ci}$. It is given by

$$S^{(1)}_{ci} := \begin{pmatrix} 0 \\ 0 \end{pmatrix}$$

for $j = 1$ and

$$S^{(2)}_{ci} := \begin{pmatrix} 0 \\ g\frac{h_{i,l}+h_{i,r}}{2}(z_{i,l} - z_{i,r}) \end{pmatrix} \tag{10}$$

for $j = 2$. Note that this corresponds to the source term discretisation (4), and below we review the argument that shows how this leads to a well-balanced scheme for the lake at rest.

Together with a second order Runge-Kutta time discretization the fully discrete second order well-balanced scheme of Audusse et al. is now complete. With constant reconstruction and without the Runge-Kutta procedure you get the associated first order scheme [1]. Audusse et al. could show for their scheme that it preserves the nonnegativity of the waterheight $h_i(t)$, it preserves the steady state of the lake at rest, is consistent with the shallow water system and there first order scheme does also satisfies an in-cell entropy inequality.

2.2. **Second order Well-Balancing.** To motivate the subsequent development of a well-balanced scheme of very high accuracy, we need to review the well-balanced property of Audusse et al.'s second order semidiscrete scheme (7).
Suppose that $H = h + z$ is constant at time t, and $u \equiv 0$. Since $H_{i,r} = H_{i+1,l}$,

$$\begin{aligned} h^*_{i,r} &= \max(0, H_{i,r} - \max(z_{i,r}, z_{i+1,l})) \\ &= \max(0, H_{i+1,l} - \max(z_{i,r}, z_{i+1,l})) \\ &= h^*_{i+1,l} \end{aligned}$$

and since $u_{i,r} = u_{i+1,l} = 0$, we also have

$$U^*_{i,r} = U^*_{i+1,l}.$$

Because now the values $U^*_{i,r}$ and $U^*_{i+1,l}$ are equal, we denote them simply by $U_{i+\frac{1}{2}}$, $h_{i+\frac{1}{2}}$, $m_{i+\frac{1}{2}} := (hu)_{i+\frac{1}{2}}$. Because $u_{i+\frac{1}{2}} = 0\ \forall i$ and by consistency of the numerical fluxes,

$$\mathcal{F}_r(U_{i+\frac{1}{2}}, U_{i+\frac{1}{2}}) = \begin{pmatrix} 0 \\ \frac{g}{2} h^2_{i+\frac{1}{2}} \end{pmatrix} \text{ and } \mathcal{F}_l(U_{i-\frac{1}{2}}, U_{i-\frac{1}{2}}) = \begin{pmatrix} 0 \\ \frac{g}{2} h^2_{i-\frac{1}{2}} \end{pmatrix}.$$

This, together with the definitions (7)–(10) of the semidiscrete scheme implies

$$\frac{d}{dt} h_i(t) = 0$$

and

$$\begin{aligned} &\frac{d}{dt} m_i \\ = \quad & -\frac{1}{\Delta x}\left[\frac{g}{2}h^2_{i+\frac{1}{2}} + \left(\frac{g}{2}h^2_{i,r} - \frac{g}{2}h^2_{i+\frac{1}{2}}\right) - \frac{g}{2}h^2_{i-\frac{1}{2}} - \left(\frac{g}{2}h^2_{i,l} - \frac{g}{2}h^2_{i-\frac{1}{2}}\right) - g\frac{h_{i,l}+h_{i,r}}{2}(z_{i,l} - z_{i,r})\right] \\ = \quad & -\frac{1}{\Delta x}\left[g\frac{h^2_{i,r} - h^2_{i,l}}{2} - g\frac{h_{i,l}+h_{i,r}}{2}((H_{i,l} - h_{i,l}) - (H_{i,r} - h_{i,r}))\right] \\ = \quad & -\frac{1}{\Delta x}\left[-g\frac{(h_{i,l}+h_{i,r})}{2}(H_{i,l} - H_{i,r})\right] \end{aligned}$$

Because of $H_{i,l} = H_{i,r} = H$,

$$\frac{d}{dt} m_i(t) = 0$$

so

$$\frac{d}{dt} U_i(t) = 0.$$

Therefore, the second order semidiscrete scheme preserves the stationary state of the lake at rest.

2.3. **Higher Order Well-Balancing.** The project of the present paper is to show how to extend the first and second order accurate well-balanced schemes to any desired order of accuracy. Most ingredients which we use are well-established in the literature: high order WENO spatial reconstructions, high order Runge-Kutta time discretizations, and appropriate quadrature rules for the initial data. But there is one essential difficulty to be solved: we need to find a quadrature rule for the source term which is both accurate and well-balanced. The remainder of this section is devoted to the solution of this question.

As before, let $U_{i,r}$, $U_{i+1,l}$ be the left and right values of a piecewise polynomial reconstruction at interface $x_{i+\frac{1}{2}}$. Of course, this time we work with polynomials of any desired order of accuracy. Define the hydrostatic reconstruction $h_{i+\frac{1}{2}\pm}$ by (5) and (6) as before, and set

$$U^*_{i,r} := \begin{pmatrix} h^*_{i,r} \\ m_{i,r} \end{pmatrix}, \quad U^*_{i+1,l} := \begin{pmatrix} h^*_{i+1,l} \\ m_{i+1,l} \end{pmatrix}. \tag{11}$$

Note that to achieve orders higher than two, it is convenient to reconstruct in the conservative variable m (which is computed with full accuracy by the finite volume scheme) instead of the primitive variable u, which is only derived from the conservative ones. We define the left and right numerical fluxes $\mathcal{F}_l$ and $\mathcal{F}_r$ by (8) and (9) as before. It remains to define a high order, well-balanced numerical quadrature of the source term

$$S := -\int_{x_{i-\frac{1}{2}}}^{x_{i+\frac{1}{2}}} ghz_x dx.$$

The main observation of this paper is that this can be done by numerical extrapolation. To do so, we subdivide each cell into N subcells and apply the quadrature (4) to all subcells. This gives the quadrature S_N,

$$S_N : g\sum_{j=1}^{N} \frac{h_{j-1}+h_j}{2}(z_{j-1}-z_j) \approx S,$$

where $z_j = z(x_{i-\frac{1}{2}} + j\Delta x/N)$ etc. are local values of the reconstruction at the interfaces of the subcells. In the situation of the lake at rest, where

$$z_{j-1} - z_j = h_j - h_{j-1}$$

the source term reduces to

$$\begin{aligned} S_N &= -\frac{g}{2}\sum_{j=1}^{N} \frac{h_{j-1}+h_j}{2}(h_j - h_{j-1}) \\ &= -\frac{g}{2}(h_N^2 - h_0^2) \\ &= -\frac{g}{2}(h_{i,r}^2 - h_{i,l}^2). \end{aligned}$$

By the same arguments as for the second order case this is well-balanced, but it is still only second order accurate (see Table 2).

To get higher orders of accuracy we use numerical extrapolation (see e.g. the textbook of Deuflhard and Bornemann [8]). Note that the quadrature (4) is symmetric and second order accurate. Therefore, from Theorem 4.39 of [8], there exists an asymptotic expansion of the form

$$S_N = S + c_1\left(\frac{\Delta x}{N}\right)^2 + c_2\left(\frac{\Delta x}{N}\right)^4 + \dots. \tag{12}$$

The S_N can be combined for different values of N to compute S with any order of accuracy. For example, to get a source term of order four, simply use

$$\frac{4S_2 - S_1}{3} = S + \tilde{c}_2(\Delta x)^4 + \dots$$

Therefore we define $S_{ci}^{(4)}$ by

(13)
$$S_{ci}^{(4)} := \frac{4\left(\frac{g}{2}(h_{l,i}+h_{c,i})(z_{l,i}-z_{c,i})+\frac{g}{2}(h_{c,i}+h_{r,i})(z_{c,i}-z_{r,i})\right)-\left(\frac{g}{2}(h_{l,i}+h_{r,i})(z_{l,i}-z_{r,i})\right)}{3}.$$

Thus for the lake at rest:

$$S_{ci}^{(4)} = -\frac{g}{2}\left(h_{i,r}^2 - h_{i,l}^2\right)$$

which leads to a well balanced scheme.

Remark 1. *Note that compared with S_1, the computation of S_2 uses only one additional reconstruction point per cell, namely the cell center. Thus we can compute S to fourth order accuracy using three points per cell, which is analogous to Simpsons rule (which may be obtained by extrapolating the trapezoidal rule). Note that we could not use Simpsons rule directly, because this would not give a well-balanced scheme.*

Remark 2. *Note that any scheme that is well balanced with the source term* (4) *will also be well balanced with the fourth order source term* (13)*.*

We summarize our high order well-balanced finite volume schemes in the following theorem:

Theorem 3. *Consider the fully discrete finite volume scheme given by a j^{th} order Runge-Kutta time discretization of the semidiscrete scheme* (7) – (9)*, with k^{th} order spatial reconstruction, hydrostatic reconstruction* (5)*,* (6)*, and* (11)*, and source term $S_{ci}^{(l)}$ given by an l^{th} order extrapolation of* (12)*. Then*

(i) the scheme preserves the stationary state of the lake at rest

(ii) the scheme is consistent of order $p := \min\{j,k,l\}$ with the shallow water equations (1)*.*

Proof. We have already proved the well-balanced property. The proof of consistency follows closely that of Theorem 3.1 of [1], q.e.d.

In the numerical experiments in Section 3, we use the classical 4^{th} order Runge-Kutta scheme, a 5^{th} order WENO reconstruction in space (see Appendix A) and the 4^{th} order extrapolation (13) of the source term. According to Theorem 3, this scheme is formally 4^{th} order accurate. Surprisingly, in experiments with smooth solutions, it clearly gives 5^{th} order convergence, see Table 1 below. Note that we could also have used Shu's TVD Runge-Kutta time discretizations [24] or the recent SSPRK schemes [13, 27].

3. Numerical Experiments

3.1. **Order of Accuracy.** To verify the order of accuracy we follow Xing and Shu [30] and choose

$$\begin{aligned} z(x) &:= \sin^2(\pi x) \\ h(x,0) &:= 5 + e^{\cos(2\pi x)} \\ hu(x,0) &:= \sin(\cos(2\pi x)) \end{aligned}$$

for bottom topography, initial water height and momentum. Here $x \in [0,1]$, the boundary conditions are periodic, and the gravitational constant g is set to 9.812. We compute up to time $t = 0.1$ with CFL number 0.4. Since the exact solution for this experiment is not known explicitly, we use the same well-balanced WENO scheme of order $(4,5,4)$ with $N = 25\,600$ cells to compute a reference solution. We use a fifth order WENO reconstruction with $\varepsilon = 10^{-6}$ and optimal weights from (31), together with the weight splitting method [23] to compute the central point values needed in the quadrature (13). Table 1 contains the L^1 errors and numerical order of accuracy for both components. We achieve full fifth order convergence in both components. Note that we have used the fifth order WENO reconstruction in space, but only a fourth order accurate extrapolation of the source term and the classical fourth order Runge-Kutta time discretization. Thus not all elements of the algorithm contribute equally to the overal error. However, a standard second order discretization of the source term does reduce the order of accuracy to two, see Table 2. This shows the relevance of the key new ingredient of our algorithm.

In the following, we will denote our well balanced WENO schemes with the triplet (j, k, l), where j, k and l denote respectively the accuracy in time of the Runge-Kutta integrator, the accuracy in space of the WENO reconstruction and the accuracy of the quadrature rule (13).

convergence table with fourth order source term

number	h		hu	
of cells	L^1 error	order	L^1 error	order
25	1.13e-02		8.22e-02	
50	1.84e-03	2.61	1.71e-02	2.27
100	2.83e-04	2.70	2.48e-03	2.78
200	2.07e-05	3.77	1.77e-04	3.81
400	8.18e-07	4.66	7.02e-06	4.66
800	2.67e-08	4.94	2.29e-07	4.94
1600	8.40e-10	4.99	7.21e-09	4.99

TABLE 1. L^1 errors and numerical orders of accuracy for Example 3.1 for the new well-balanced finite volume scheme of order $(4, 5, 4)$.

convergence table with second order source term

number	h		hu	
of cells	L^1 error	order	L^1 error	order
25	1.12e-02		8.29e-02	
50	1.87e-03	2.58	1.73e-02	2.27
100	2.86e-04	2.71	2.50e-03	2.78
200	2.18e-05	3.70	1.82e-04	3.77
400	1.37e-06	3.99	9.99e-06	4.19
800	2.18e-07	2.65	1.46e-06	2.77
1600	5.05e-08	2.11	3.31e-07	2.14

TABLE 2. Same as Table 1, but second order discretization of the source term S_{ci} (order $(4, 5, 2)$).

3.2. **Perturbation of a lake at rest.** The following problem was studied by LeVeque [21]. It shows the behavior of a small perturbation of a lake at rest with variable bottom topography

$$z(x) = \begin{cases} 0.25(1 + cos(10\pi(x - 0.5))), & \text{if } 1.2 \leq x \leq 1.4 \\ 0, & \text{else} \end{cases}$$

where $x \in [0, 2]$. The total initial height is given by

$$H(x, 0) = \begin{cases} 1 + \Delta H, & \text{if } 1.1 \leq x \leq 1.2 \\ 1, & \text{else} \end{cases}$$

LeVeque, who worked with a second order scheme, used $\Delta H = 0.1$. Xing and Shu [30], Vukovic and Sopta [29] and we use higher order schemes, and here we test $\Delta H = 0.001$. The initial velocity is set to

$$v(x, 0) = 0$$

and the gravitational constant $g = 9.81$. We use a fifth order WENO reconstruction with optimal weights from (31) and $\varepsilon = 10^{-12}$ in order to satisfy (33). Indeed, $\varepsilon = 10^{-6}$ results in oscillations at the shocks. Periodic boundary conditions are used. The CFL number is 0.4 and the final time is $T = 0.2$.

Figures 5 and 6 show total height and momentum computed with 200 cells and 157 timesteps, and a comparison between first, second and $(4, 5, 4)^{th}$ order solutions are shown in Figure 7. At this time, the wave travelling to the right has just passed the hump, and part of it has been reflected. All the schemes are able to produce the physically correct reflected waves (see the interval $[1, 1.5]$ around the hump). The new scheme shows remarkably high resolution. Schemes which do not preserve the discrete hydrostatic balance may introduce unphysical waves and high frequency oscillations (see [29, Figure 8 & 9]).

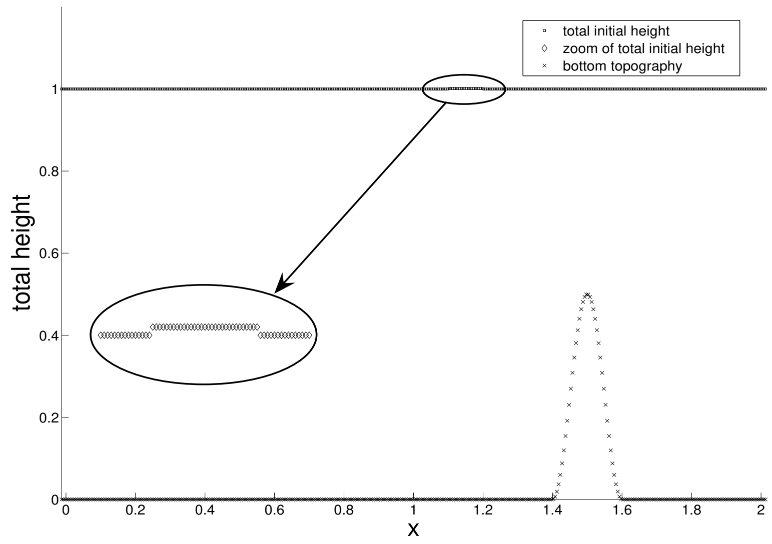

FIGURE 4. Example 3.2, bottom topography and initial water level.

3.3. **Dambreak over a rectangular wall.** This test case simulates a dambreak over a rectangular wall. It produces a rapidly varying flow over a discontinuous bottom topography. This example was used in [29],[30]. The bottom topography is given by

$$z(x) = \begin{cases} 8, & \text{if } |x - 1500/2| \leq 1500/8 \\ 0, & \text{otherwise,} \end{cases}$$

with $x \in [0, 1500]$. The total initial height is

$$H(x, 0) = \begin{cases} 20, & \text{if } 0 \leq x \leq 750 \\ 15, & \text{otherwise.} \end{cases}$$

The initial velocity is set to zero $v(x, 0) = 0$ and the gravitation constant is $g = 9.81$. At the left boundary we use reflective boundary conditions and on the right side open boundary

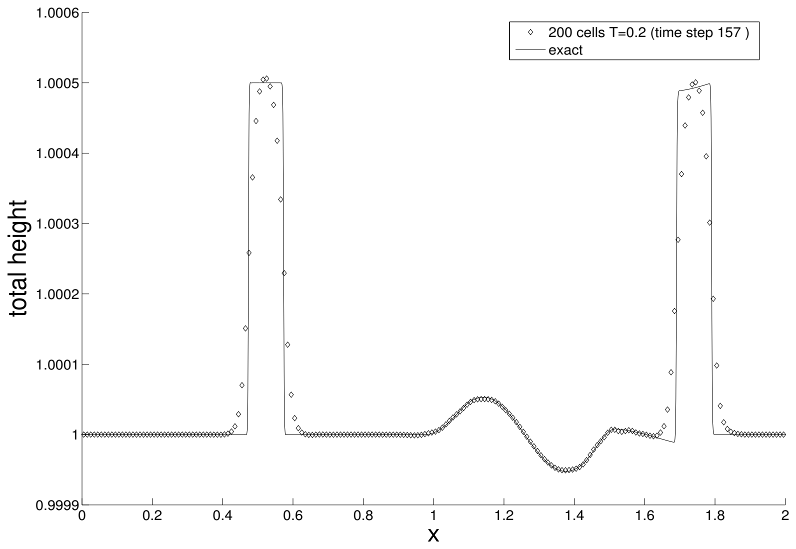

FIGURE 5. Example 3.2, total height at $T = 0.2$ computed with 200 cells.

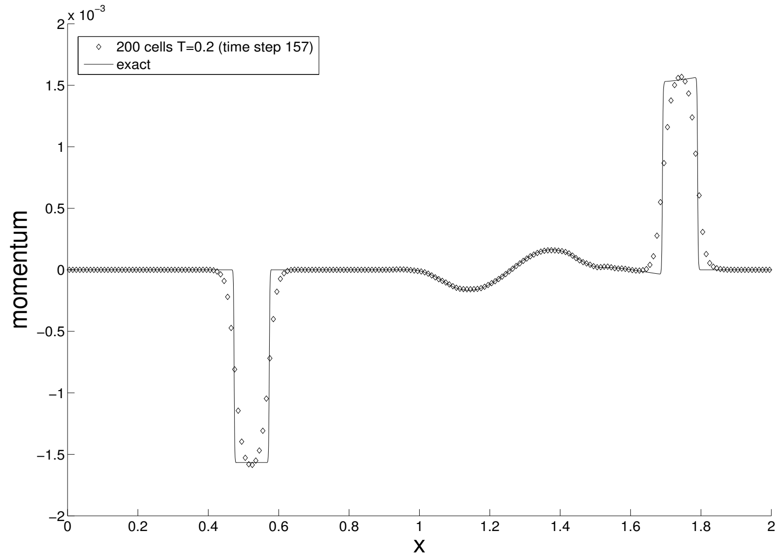

FIGURE 6. Example 3.2, momentum at $T = 0.2$ computed with 200 cells.

conditions. In Figure 8 we show level lines of the water level, or total height, of the solution up to time $T = 60$. In the beginning, one observes the standard rarefaction and shock waves which form the solution of the Riemann problem of the homogeneous shallow water equations. Figures 9 and 10 show the water level and velocity at $T = 15$. At time $T \approx 17$ the waves cross the two edges of the wall. A part is transmitted, another part reflected, and a remaining part becomes a standing wave. Such standing waves have recently been studied analytically by Klausen and Risebro [18], Towers [28], Klingenberg and Risebro [19], and Seguin and Vovelle [22] who consider the inhomogeneous one dimensional shallow water equations as a system of three conservation laws for (h, hu, z) with $\partial_t z = 0$. This system has the three wave speeds

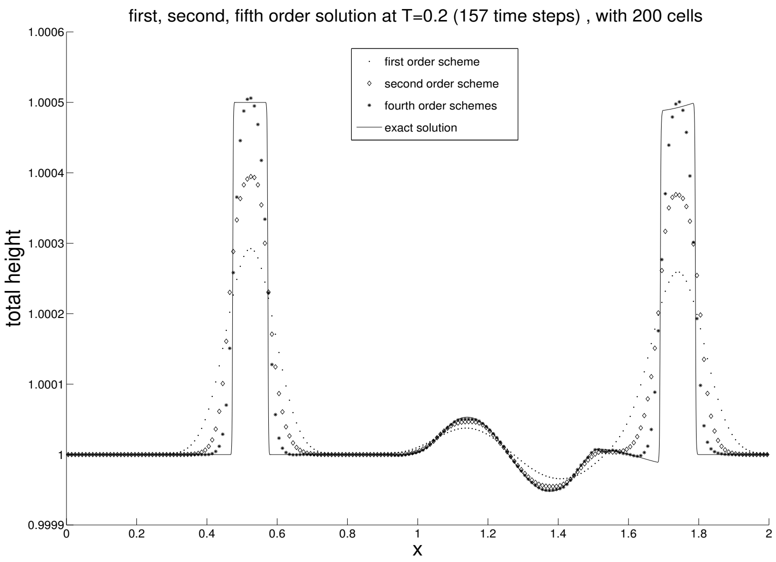

FIGURE 7. Example 3.2, total height at $T = 0.2$ computed with first, second, and $(4,5,4)^{th}$ order schemes and 200 cells.

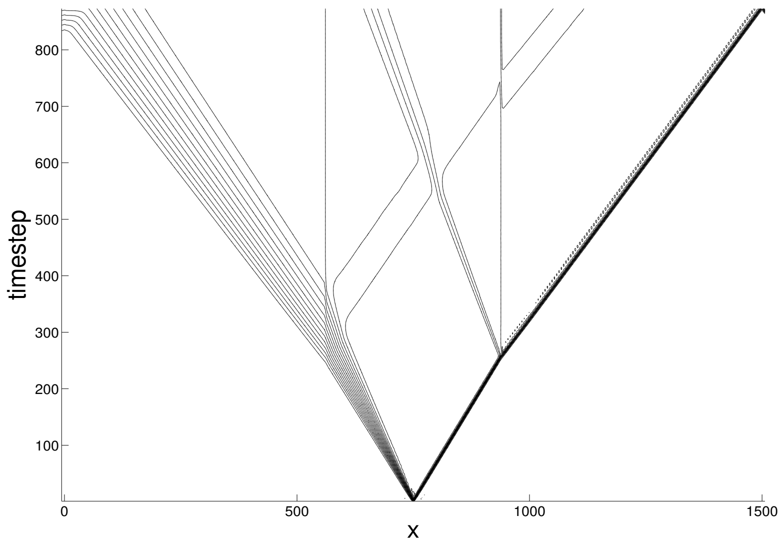

FIGURE 8. Example 3.3, contourplot of water level in the $x - t$ plane.

$u \pm \sqrt{gh}$ and 0. For later times, the wave system keeps interacting. At time $T = 60$, we have six waves in the solution. The main shock and rarefaction waves just hit the boundary of the computational domain. Between them we have, from left to right, a standing wave, a weak rarefaction travelling leftwards, a second standing wave, and a weak compressive wave travelling rightwards. Figures 11 and 12 show cross sections of total height and velocity. Note that the standing waves are not easy to capture, even by a high resolution method as the one proposed in [29]. Here we have almost perfect resolution of all features of this challenging solution.

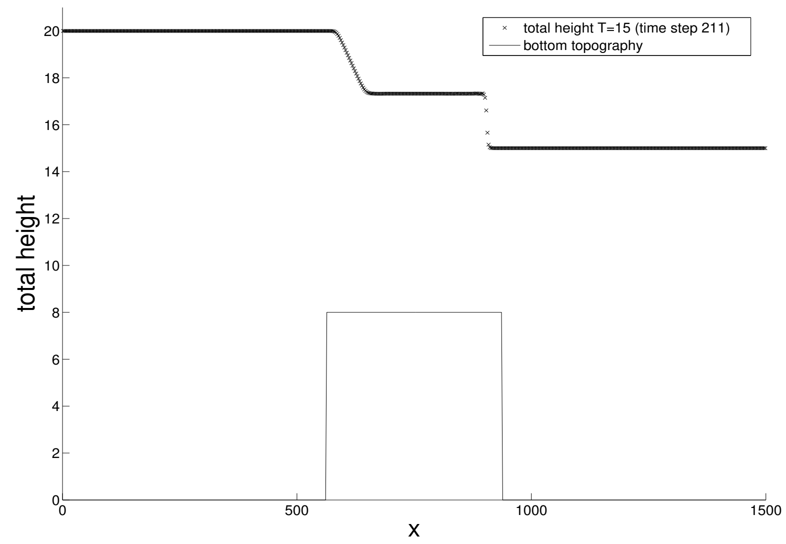

FIGURE 9. Example 3.3, water level at $T = 15$, 600 cells.

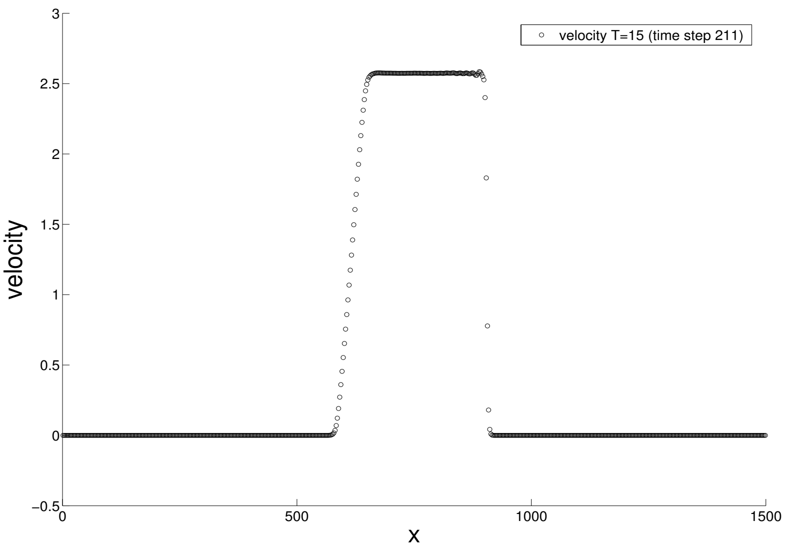

FIGURE 10. Example 3.3, velocity at $T = 15$, 600 cells.

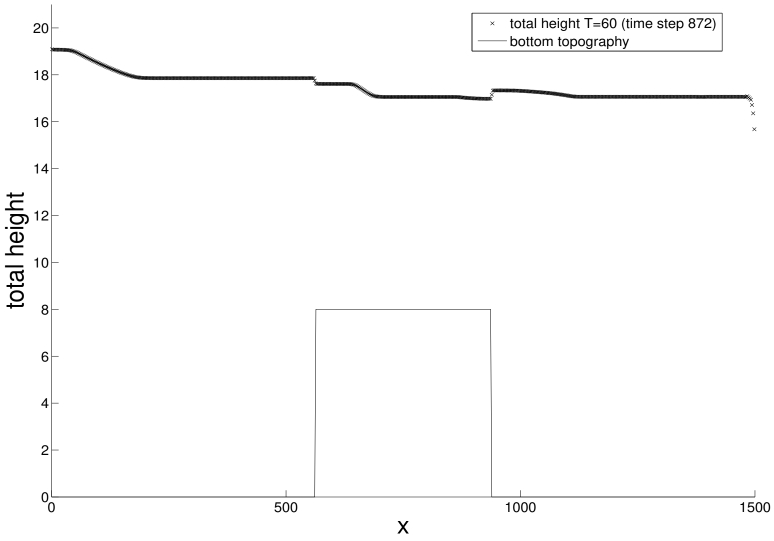

FIGURE 11. Example 3.3, water level at $T = 60$, 600 cells.

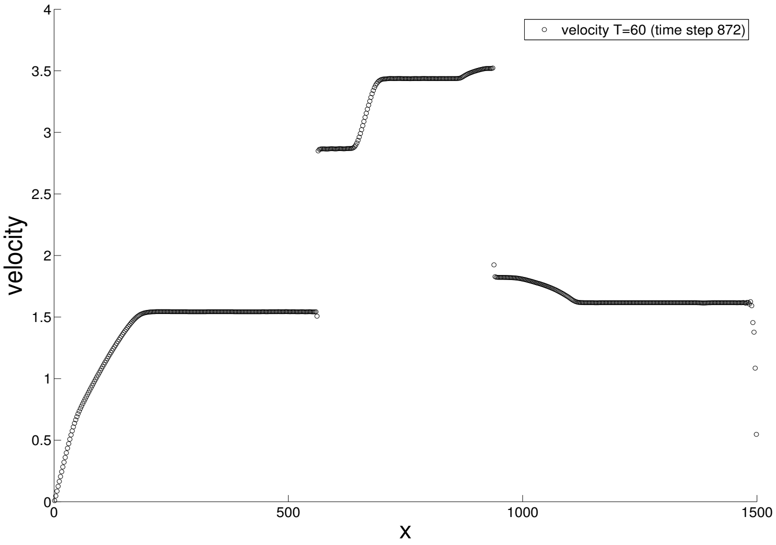

FIGURE 12. Example 3.3, velocity at $T = 60$, 600 cells.

4. Two dimensional extension

The shallow water equations in 2D are given by

$$\begin{aligned} h_t + (hu)_x + (hv)_y &= 0 \\ (hu)_t + \left(hu^2 + \tfrac{1}{2}gh^2\right)_x + (huv)_y &= -ghz_x \\ (hv)_t + (huv)_x + \left(hv^2 + \tfrac{1}{2}gh^2\right)_y &= -ghz_y, \end{aligned} \tag{14}$$

where h is the water height, z is the bottom topography, u is the velocity in x-direction, v is the velocity in y-direction and g is the gravitational constant. We will now discuss how to extend our scheme to two dimensions.

4.1. **Overview of the scheme.** Rewrite the system (14) in the standard form:

$$U_t + F_x(U) + G_y(U) = S(U), \tag{15}$$

where clearly $U = (h, hu, hv)^T$, $F = (hu, hu^2 + \frac{1}{2}gh^2, huv)^T$, $G = (hv, huv, hv^2 + \frac{1}{2}gh^2)^T$ and $S = (0, -ghz_x, -ghz_y)^T$. We define the cell averages over grid cells $I_{ij} = (x_{i-\frac{1}{2}}, x_{i+\frac{1}{2}}) \times (y_{j-\frac{1}{2}}, y_{j+\frac{1}{2}})$ by

$$U_{ij} = \frac{1}{\Delta x \Delta y} \int_{I_{ij}} U(x,y)dxdy, \tag{16}$$

where $\Delta x = x_{i+\frac{1}{2}} - x_{i-\frac{1}{2}}$, $\Delta y = y_{j+\frac{1}{2}} - y_{j-\frac{1}{2}}$. Suppose for simplicity that the cells are square: let $\delta = \Delta x = \Delta y$. Integrating each term in (14) over the cell I_{ij} and invoking the divergence theorem, we get the following semidiscrete scheme for the evolution of the cell averages U_{ij}:

$$\delta^2 \frac{d}{dt} U_{ij}(t) + \int_{\partial I_{ij}} (F,G) \cdot \mathbf{n} \mathrm{d}s = \int_{I_{ij}} S \mathrm{d}x\mathrm{d}y,$$

Rewrite the system as:

$$\frac{d}{dt} U_{ij}(t) + \frac{\bar{F}_{i+\frac{1}{2},j} - \bar{F}_{i-\frac{1}{2},j}}{\delta} + \frac{\bar{G}_{i,j+\frac{1}{2}} - \bar{G}_{i,j-\frac{1}{2}}}{\delta} = S_{ij} \tag{17}$$

where

$$\bar{F}_{i-\frac{1}{2},j} = \frac{1}{\delta} \int_{y_j - \frac{1}{2}\delta}^{y_j + \frac{1}{2}\delta} F(U(x_{i-\frac{1}{2}}, y))\, dy \tag{18}$$

$$\bar{G}_{i,j-\frac{1}{2}} = \frac{1}{\delta} \int_{x_i - \frac{1}{2}\delta}^{x_i + \frac{1}{2}\delta} G(U(x, y_{j-\frac{1}{2}}))\, dx \tag{19}$$

$$S_{ij} = \frac{1}{\delta^2} \int_{I_{ij}} S(x,y)\, dx\, dy; \tag{20}$$

In analogy with the 1D case, we reconstruct the variables h, hu, hv, and H, while the bottom topography is given by $z = H - h$. In general, this yields a discontinuous approximation of z. Let $U_{ij}(x,y)$ denote the reconstruction computed in the cell I_{ij} with U denoting any of the reconstructed variables. Again, to preserve the equilibrium states, a hydrostatic reconstruction is needed on the quadrature points on the boundary of the cell, which will be denoted by h^*:

$$\begin{aligned}
h^*_{i+1,j}(x^+_{i+\frac{1}{2}},\cdot) &= \max\left(0, H_{i+1,j}(x_{i+\frac{1}{2}},\cdot) - \max\left(z_{ij}(x_{i+\frac{1}{2}},\cdot), z_{i+1,j}(x_{i+\frac{1}{2}},\cdot)\right)\right),\\
h^*_{ij}(x^-_{i+\frac{1}{2}},\cdot) &= \max\left(0, H_{ij}(x_{i+\frac{1}{2}},\cdot) - \max\left(z_{ij}(x_{i+\frac{1}{2}},\cdot), z_{i+1,j}(x_{i+\frac{1}{2}},\cdot)\right)\right),\\
h^*_{i,j+1}(\cdot,y^+_{j+\frac{1}{2}}) &= \max\left(0, H_{i,j+1}(\cdot,y_{j+\frac{1}{2}}) - \max\left(z_{ij}(\cdot,y_{j+\frac{1}{2}}), z_{i,j+1}(\cdot,x_{j+\frac{1}{2}})\right)\right),\\
h^*_{ij}(\cdot,y^-_{j+\frac{1}{2}}) &= \max\left(0, H_{ij}(\cdot,y_{j+\frac{1}{2}}) - \max\left(z_{ij}(\cdot,y_{j+\frac{1}{2}}), z_{i,j+1}(\cdot,y_{j+\frac{1}{2}})\right)\right).
\end{aligned}$$

To approximate the quantities $\bar{F}_{i-\frac{1}{2},j}$ and $\bar{G}_{i,j-\frac{1}{2}}$ in (18) and (19), we use a quadrature

$$\bar{F}_{i-\frac{1}{2},j} \simeq \sum_k \omega_k F(U(x_{i-\frac{1}{2}}, y_j + \xi_k\delta)),$$

where ω_k and ξ_k are the weights and nodes of the quadrature formula. For a fourth order scheme we use the classical two-point Gaussian formula

$$\bar{F}_{i-\frac{1}{2},j} \simeq \frac{1}{2}\left(F(U(x_{i-\frac{1}{2}}, y_j - \alpha\delta)) + F(U(x_{i-\frac{1}{2}}, y_j + \alpha\delta))\right), \tag{21}$$

where $\alpha = 1/(2\sqrt{3})$. A similar formula holds for $\bar{G}_{i,j-\frac{1}{2}}$.

We still need to construct a well balanced approximation to each of the flux evaluations required in (21). As in 1D, the numerical flux is composed of two contributions. The first contribution (F^h for F and G^h for G) is consistent with the flux of the homogeneous shallow water equations, the second contribution compensates the perturbation introduced by the hydrostatic correction.

The modified state variables that will be applied in the flux computations are

$$U^*_{ij} = \begin{pmatrix} h^*_{ij} \\ (hu)_{ij} \\ (hv)_{ij} \end{pmatrix}.$$

Along the edge $(x_{i-\frac{1}{2}}, y)$ for instance the numerical fluxes are

$$\begin{aligned}
\mathcal{F}^l(U^*,z)_{i-\frac{1}{2},j\pm\alpha} := {}& F^h(U^*_{i-1,j}(x_{i-\frac{1}{2}}, y_j \pm \alpha\delta), U^*_{ij}(x_{i-\frac{1}{2}}, y_j \pm \alpha\delta))\\
&+ \frac{g}{2}\begin{pmatrix} 0 \\ h^2_{ij}(x_{i-\frac{1}{2}}, y_j \pm \alpha\delta) - (h^*)^2_{ij}(x_{i-\frac{1}{2}}, y_j \pm \alpha\delta) \\ 0 \end{pmatrix}
\end{aligned} \tag{22}$$

and

$$\begin{aligned}
\mathcal{F}^r(U^*,z)_{i+\frac{1}{2},j\pm\alpha} := {}& F^h(U^*_{i,j}(x_{i+\frac{1}{2}}, y_j \pm \alpha\delta), U^*_{i+1,j}(x_{i+\frac{1}{2}}, y_j \pm \alpha\delta))\\
&+ \frac{g}{2}\begin{pmatrix} 0 \\ h^2_{ij}(x_{i+\frac{1}{2}}, y_j \pm \alpha\delta) - (h^*)^2_{ij}(x_{i+\frac{1}{2}}, y_j \pm \alpha\delta) \\ 0 \end{pmatrix},
\end{aligned} \tag{23}$$

with similar formulas for $\mathcal{G}^l$ and $\mathcal{G}^r$.

Thus the semidiscrete scheme can be written as,

$$\begin{aligned}
\frac{d}{dt}U_{ij}(t) = -\frac{1}{2\delta}\Big(&\mathcal{F}^r_{i+\frac{1}{2},j+\alpha} + \mathcal{F}^r_{i+\frac{1}{2},j-\alpha} - \mathcal{F}^l_{i-\frac{1}{2},j+\alpha} - \mathcal{F}^l_{i-\frac{1}{2},j-\alpha}\\
&\mathcal{G}^r_{i+\alpha,j+\frac{1}{2}} + \mathcal{G}^r_{i-\alpha,j+\frac{1}{2}} - \mathcal{G}^l_{i+\alpha,j-\frac{1}{2}} - \mathcal{G}^l_{i-\alpha,j-\frac{1}{2}}\Big) + S_{ij}.
\end{aligned} \tag{24}$$

The construction of the source term S_{ij} is carried out as follows. First we write the source term componentwise: $S_{ij} = (0, S^x_{ij}, S^y_{ij})^T$. Note that the component of the source term in the x-momentum equation contains only the derivative of z along the x direction. Thus, we employ the well-balanced quadrature (13) of the previous section to integrate in the x-direction and apply the Gaussian rule in the y-direction. For the fourth order case,

$$S^x_{ij} = \frac{\delta}{2}\left(s^x_i(y_j + \alpha\delta) + s^x_i(y_j - \alpha\delta)\right), \tag{25}$$

where,

$$\begin{aligned} s^x_i(y) = \frac{4g}{6}&((h_{ij}(x_{i-\frac{1}{2}}, y) + h_{ij}(x_i, y))(z_{ij}(x_{i-\frac{1}{2}}, y) - z_{ij}(x_i, y)) \\ &+ (h_{ij}(x_i, y) + h_{ij}(x_{i+\frac{1}{2}}, y))(z_{ij}(x_i, y) - z_{ij}(x_{i+\frac{1}{2}}, y))) \\ &- \frac{g}{6}(h_{ij}(x_{i-\frac{1}{2}}, y) + h_{ij}(x_{i+\frac{1}{2}}, y))(z_{ij}(x_{i-\frac{1}{2}}, y) - z_{ij}(x_{i+\frac{1}{2}}, y)). \end{aligned}$$

In the same fashion, we compute the source S^y_{ij} using (13) in the y-direction and the Gaussian rule in the x-direction. Again, in the fourth order case:

$$S^y_{ij} = \frac{\delta}{2}\left(s^y_j(x_i + \alpha\delta) + s^y_j(x_i - \alpha\delta)\right), \tag{26}$$

where now,

$$\begin{aligned} s^y_j(x) = \frac{4g}{6}&((h_{ij}(x, y_{j-\frac{1}{2}}) + h_{ij}(x, y_j))(z_{ij}(x, y_{j-\frac{1}{2}}) - z_{ij}(x, y_j)) \\ &+ (h_{ij}(x, y_j) + h_{ij}(x, y_{j+\frac{1}{2}}))(z_{ij}(x, y_j) - z_{ij}(x, y_{j+\frac{1}{2}}))) \\ &- \frac{g}{6}(h_{ij}(x, y_{j-\frac{1}{2}}) + h_{ij}(x, y_{j+\frac{1}{2}}))(z_{ij}(x, y_{j-\frac{1}{2}}) - z_{ij}(x, y_{j+\frac{1}{2}})). \end{aligned}$$

Using the same arguments as in the proof of Theorem 3 one can show:

Corollary 4. *The 2D scheme is fourth order accurate and preserves the stationary state of the lake at rest.*

4.2. **2D reconstruction.** In order to evaluate the numerical flux functions $\mathcal{F}$ and $\mathcal{G}$ and the source term S, we need to reconstruct pointvalues of H, h, hu and hv at 12 integration points, 8 on the boundary $(x_{i\pm\frac{1}{2}}, y_{j\pm\alpha})$, $(x_{i\pm\alpha}, y_{j\pm\frac{1}{2}})$ and 4 in the interior $(x_i, y_{j\pm\alpha})$ and $(x_{i\pm\alpha}, y_j)$ as shown on the right of Figure 13. Note that the interior points are required only to compute the source term, which is fourth order accurate. As in the 1D case we apply a WENO procedure to find these data.

In 2D this reconstruction is somewhat more involved. Our approach is to reconstruct each variable dimension by dimension. For each cell, the one dimensional WENO procedure has to be applied six times to produce pointvalues in all quadrature points.

To fix ideas, we illustrate the algorithm for the reconstruction of the variable h. In this section only, we denote the cell averages as $\bar{\bar{h}}_{ij}$, to distinguish the averages computed on a cell (a double integral) from the averages computed along only one segment (a single integral).

We start applying the WENO reconstruction procedure in the y direction, starting from the cell averages $\bar{\bar{h}}_{ij}$. We apply the reconstruction defined by the constants in Appendix A (32) and we find approximations in the points $(x_i, y_{j+\alpha})$ and $(x_i, y_{j-\alpha})$ to the function:

$$\bar{h}_{ij}(x_i, y_{j\pm\alpha}) = \frac{1}{\delta}\int_{x_i-\frac{\delta}{2}}^{x_i+\frac{\delta}{2}} h(x, y_{j\pm\alpha})\, dx.$$

Once these data are available for all i, we apply again the WENO reconstruction along the x axis to get the required pointvalues, i.e. $h_{ij}(x_{i-\frac{1}{2}}, y_{j+\alpha})$, $h_{ij}(x_i, y_{j+\alpha})$ and $h_{ij}(x_{i+\frac{1}{2}}, y_{j+\alpha})$, starting from $\bar{h}_{ij}(x_i, y_{j+\alpha})$. With another reconstruction, we find $h_{ij}(x_{i-\frac{1}{2}}, y_{j-\alpha})$, $h_{ij}(x_i, y_{j-\alpha})$ and $h_{ij}(x_{i+\frac{1}{2}}, y_{j-\alpha})$, starting from $\bar{h}_{ij}(x_i, y_{j-\alpha})$. This set of operations will be called yx sweep, see Figure 14.

To get the quadrature points along the dashed lines on the right in Figure 13, we perform the same operations in the reversed order. This will be called x-y sweep, see Figure 15.

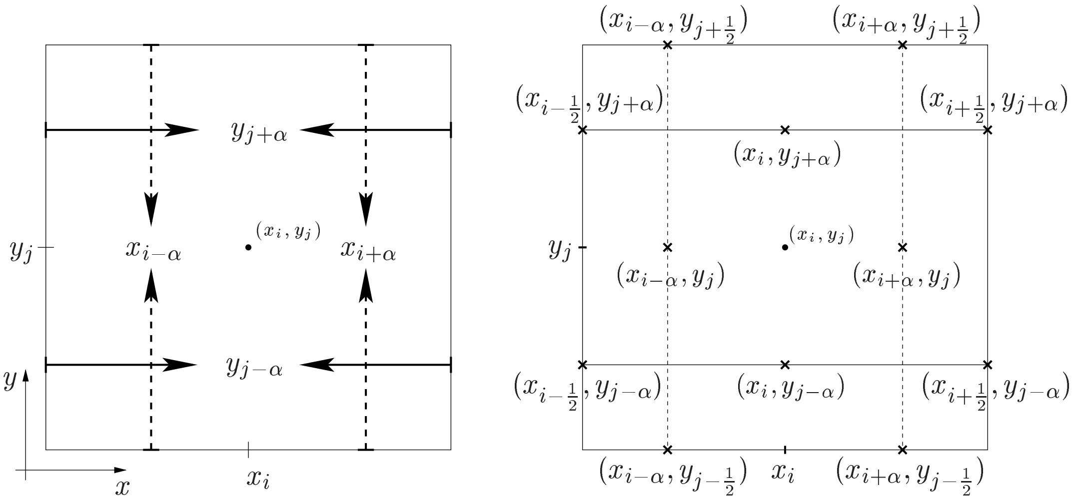

FIGURE 13. (Left) The positions of the reconstructed crosssection averages $(x_{i\pm\alpha}, \cdot)$ (dashed lines), $(\cdot, y_{j\pm\alpha})$ (black lines) for the first reconstruction step. (Right) The Gaussian integration points for the edges $(x_{i\pm\frac{1}{2}}, y_{j\pm\alpha})$, $(x_{i\pm\alpha}, y_{j\pm\frac{1}{2}})$ and for the interior, $(x_i, y_{j\pm\alpha})$ and $(x_{i\pm\alpha}, y_j)$. The point values in these locations are computed in the second step of the reconstruction.

Now, all the quantities appearing in the semidiscrete scheme (17) have been defined. Finally, to get a fully discrete scheme, we need to specify a method to march forward in time. As in the 1D scheme, we apply the classic fourth order Runge-Kutta method. For other cases, it might be advantageous to use the recent TVD or SSP Runge-Kutta schemes [24, 13, 27].

4.3. **Well-balanced test in two dimensions.** The two dimensional experiments we present here follow closely the work of Xing and Shu [30]. We check the behavior of the two dimensional scheme in a lake at rest situation on a rectangular domain $[0, 1] \times [0, 1]$, with a non-flat bottom topography

$$z(x, y) = 0.8e^{-50\left((x-0.5)^2+(y-0.5)^2\right)}. \tag{27}$$

The initial water height is

$$h(x, y) = 1 - z(x, y), \tag{28}$$

so that the water surface level H is constant 1.0. The momentum in x and y direction is set to zero:

$$hu(x, y, t = 0) = 0 \text{ and } hv(x, y, t = 0) = 0. \tag{29}$$

The lake is at rest initially, and should remain at rest indefinitely. In this situation, a scheme without well-balancing would produce unphysical waves. For this test we use a uniform

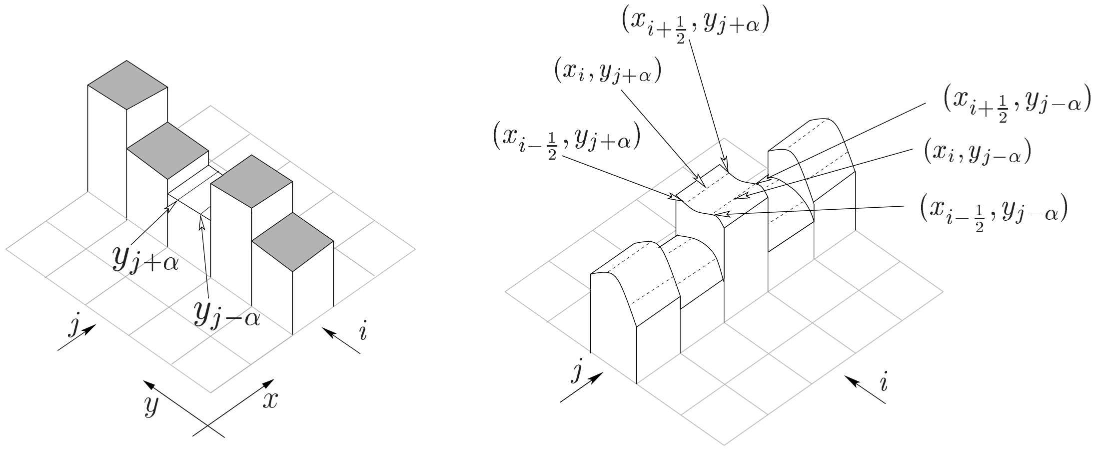

FIGURE 14. In the first step of the y-x-sweep we compute averages over crossections $(\cdot, y_{j\pm\alpha})$ marked with black lines in the figure on the left side. In the second step of the y-x-sweep we use the crossection averages to compute point values at quadrature points $(x_{i\pm\frac{1}{2}}, y_{j\pm\alpha})$, $(x_i, y_{j\pm\alpha})$ (right figure).

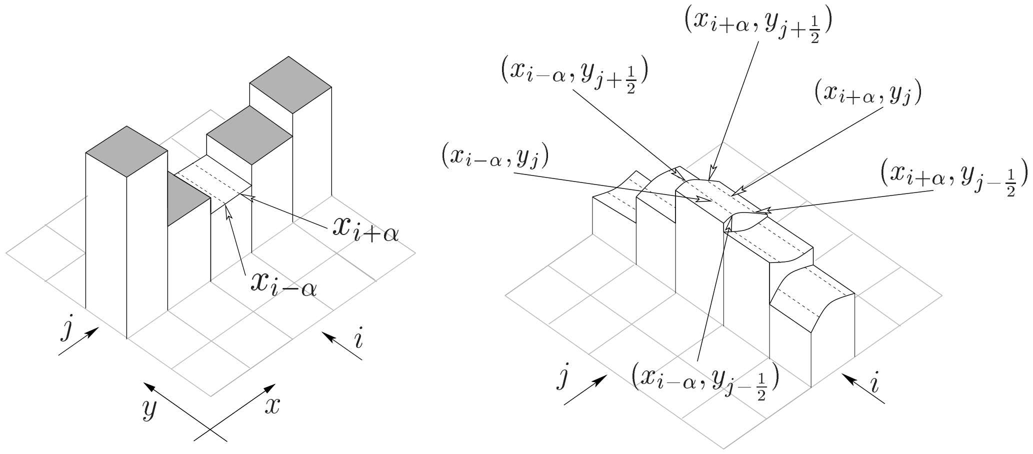

FIGURE 15. In the first step of the x-y-sweep we compute averages over crossections $(\cdot, x_{i\pm\alpha})$ marked with dotted lines in the figure on the left side. In the second step of the x-y-sweep we use the crossection averages to compute point values at quadrature points $(x_{i\pm\alpha}, y_{j\pm\frac{1}{2}})$ $(x_{i\pm\alpha}, y_j)$ (right figure).

100×100 grid and compute the solution at time $t = 0.1$. We get following L^1-errors for the conservative components: $||h||_1 = 1.23e^{-16}$, $||hu||_1 = 2.20e^{-16}$ and $||hv||_1 = 2.22e^{-16}$. The errors are all of the magnitude of the rounding error e^{-16} thus the scheme is indeed perfectly well-balanced.

number of points	CFL	h		hu		hv	
		L^1 error	order	L^1 error	order	L^1 error	order
25	0.5	8.77-03		3.42e-02		6.71e-02	
50	0.5	1.10e-03	3.00	2.73e-03	3.65	9.40e-03	2.84
100	0.5	9.84e-05	3.48	1.56e-04	4.13	7.85e-04	3.58
200	0.5	4.91e-06	4.32	6.58e-06	4.57	3.93e-05	4.32
400	0.5	1.82e-07	4.76	2.41e-07	4.77	1.46e-06	4.75
800	0.5	6.06e-09	4.91	7.94e-09	4.92	4.90e-08	4.90

TABLE 3. L^1-errors and numerical order of accuracy for the convergence test 4.4

4.4. **Testing the order of accuracy.** To check the numerical order of accuracy we use the same experiment as Xing and Shu [30]. On the unit square $[0,1]\times[0,1]$ we choose the bottom topography:

$$z(x,y) = \sin(2\pi x) + \cos(2\pi y)$$

the initial water surface level:

$$h(x,y,t=0) = 10 + e^{\sin(2\pi x)}\cos(2\pi y)$$

and the initial momentum in the x and y directions respectively:

$$hu(x,y,t=0) = \sin(\cos(2\pi x))\,\sin(2\pi y)$$
$$hv(x,y,t=0) = \cos(2\pi x)\,\cos(\sin(2\pi y)).$$

We compute up to time $T = 0.05$ with CFL-number 0.8. For the WENO reconstruction we use the optimal weights of (31),(32) and set $\varepsilon = 10^{-6}$. The reference solution is computed with the same scheme and 1600×1600 cells, since the exact solution is unknown.
For this experiment we expect fourth order of accuracy in all conservative components. The applied standard Runge-Kutta time integration, the integration of the numerical fluxes with Gaussian rule and the cell centered source term are all formally fourth order accurate, while the applied WENO reconstruction is fifth order accurate. Table 3 contains the L^1-errors and orders of accuracy. We can clearly see that for this two dimensional test case, fourth order accuracy (in fact almost fifth order) is indeed achieved in all components.

4.5. **A small Pertubation of a Two Dimensional Steady-State Water.** This classical problem is given by LeVeque [21] and is also computed in [30]. For this problem we consider the rectangular domain $[0,2]\times[0,1]$. The bottom topography is displayed in Figure 16 and it is given by:

$$z(x,y) = 0.8e^{\left(-5(x-0.9)^2-50(y-0.5)^2\right)}.$$

The initial water surface level is given by:

$$h(x,y,t=0) = \begin{cases} 1.01 - z(x,y) & \text{if } 0.05 \le x \le 0.15 \\ 1 - z(x,y) & \text{otherwise} \end{cases},$$

so the initial surface level is almost flat, only in the region $0.05 < x < 0.15$ it is perturbed upward by the displacement 0.01. The initial momentum in the x and y directions is:

$$hu(x,y,t=0) = 0$$
$$hv(x,y,t=0) = 0.$$

We compute using two different uniform meshes with 200×100 cells and 600×300 cells.
Figure 17 shows 30 uniformly spaced contour lines of the surface level H at times $t = 0.12,\ 0.24,\ 0.36,\ 0.48$ and final time $T = 0.6$. The results obtained with the course grid

appear on the left side, while on the right we find the numerical solution obtained with the fine grid.
In the simulation with the coarse grid we use $\varepsilon = 10^{-6}$ and for the fine grid $\varepsilon = 10^{-9}$. In both experiments we choose the CFL-number equal to 0.5. As we can see, we get results comparable to the finite difference approach in [30].

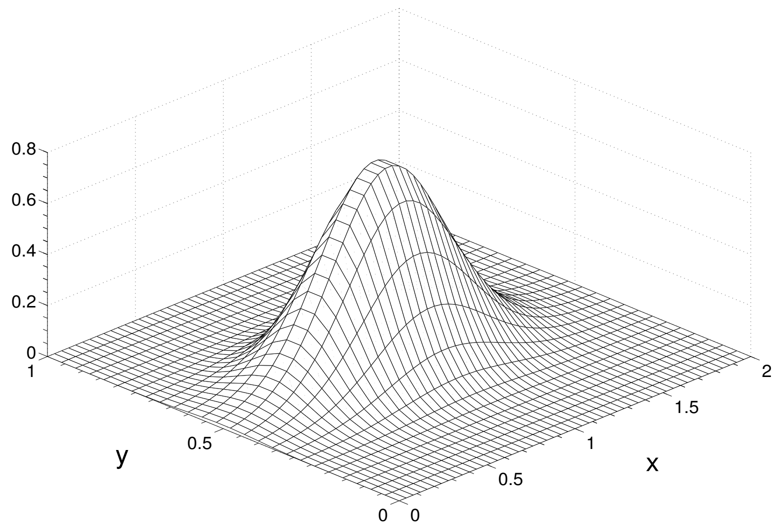

FIGURE 16. Bottom topography of experiment 4.5 $z(x, y) = 0.8e^{\left(-5(x-0.9)^2-50(y-0.5)^2\right)}$.

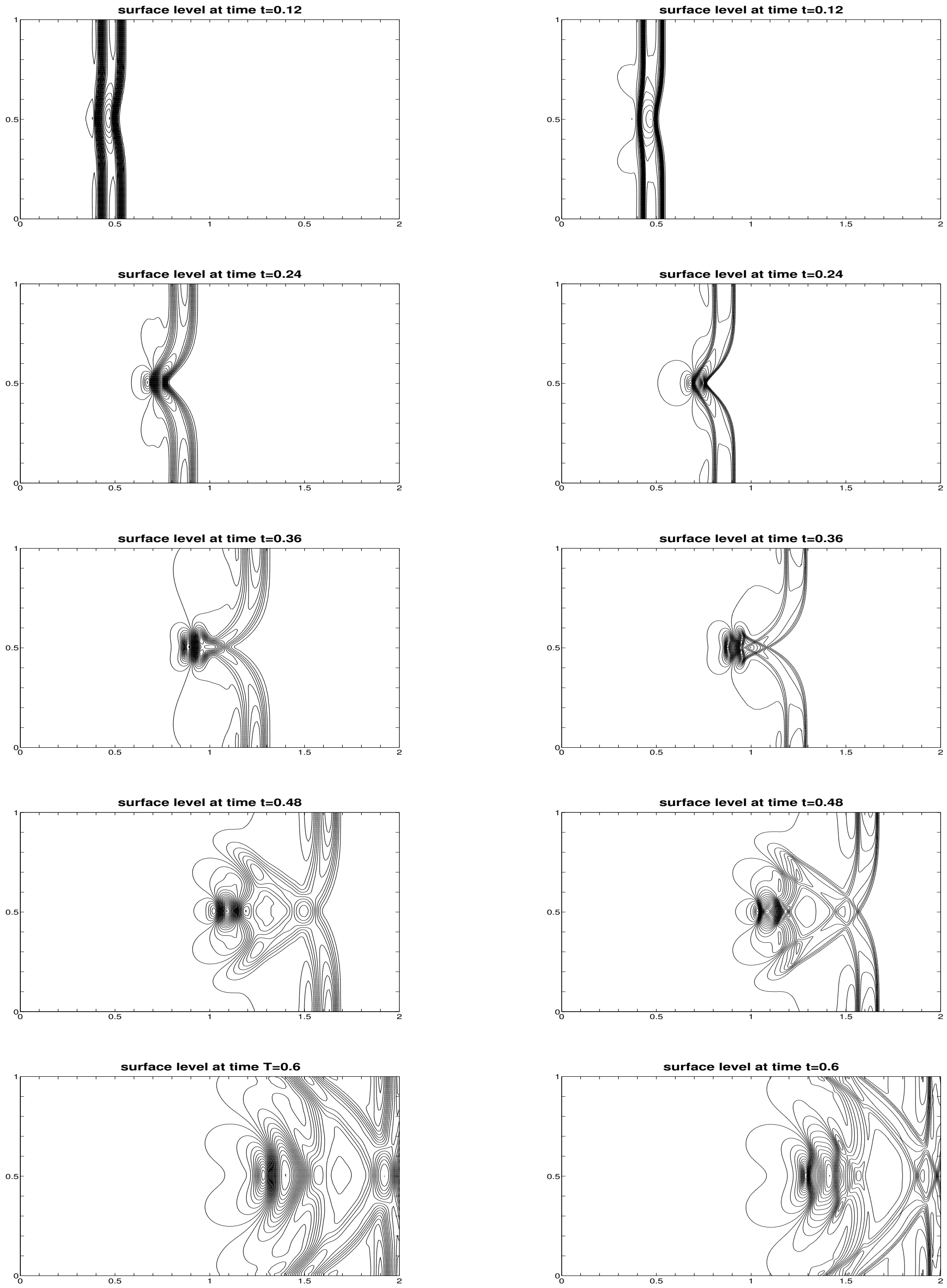

FIGURE 17. Contour lines of the surface level $h + z$ for the experiment of Subsection 4.5 at times $t = 0.12, 0.24, 0.36, 0.48, 0.6$. Left: 200×100 grid, right: 600×300 grid. There are 30 uniformly spaced contour lines in each plot. At time $t = 0.12$ the contour lines go from 0.999837 to 1.005974; at time $t = 0.24$ from 0.996091 to 1.014523; at time $t = 0.36$ from 0.988829 to 1.011245; at time $t = 0.48$ from 0.990559 to 1.004614; at time $t = 0.6$ from 0.995244 to 1.005207.

5. Conclusion

In this paper, we have constructed well-balanced finite volume schemes for the shallow water equations, which are of any desired order of accuracy. The new schemes generalize a class of second order schemes proposed by Audusse et al. [1]. A $(4,5,4)^{th}$ order version of the new scheme gives the expected high resolution both for smooth and non-smooth flows, and perfect balance for the lake at rest in one and two spatial directions. The key technique, a new quadrature formula for the source term, can be applied to a wide variety of first and second order well balanced schemes, to raise their order of accuracy. Work on stable schemes for flows with dry areas is in progress.

References

[1] E. Audusse, F. Bouchut, M.-O. Bristeau, R. Klein, B. Perthame, A fast and stable well-balanced scheme with hydrostatic reconstruction for shallow water flows, SIAM J. Sci. Comp. 25, (2004), 2050-2065.
[2] D. S. Bale, R. J. LeVeque, S. Mitran, and J. A. Rossmanith, A Wave Propagation Method for Conservation Laws and Balance Laws with Spatially Varying Flux Functions, SIAM J. Sci. Comp. 24, (2002), 955-978.
[3] A. Bermudez and M.E. Vazquez, Upwind methods for hyperbolic conservation laws with source terms, Computers and Fluids 23, (1994) 1049-1971.
[4] N. Botta, R. Klein, S. Langenberg and S. Lützenkirchen, Well-balanced finite volume methods for nearly hydrostatic flows, J. Comp. Phys. Vol. 196, (2004), 539-565.
[5] F. Bouchut, A. Mangeney-Castelnau, B. Perthame, J.-P. Vilotte, A new model of Saint Venant and Savage-Hutter type for gravity driven shallow water flows, C.R. Acad. Sci. Paris, série I 336 (2003), 531-536.
[6] F. Bouchut, J. Le Sommer, V. Zeitlin, Frontal geostrophic adjustment and nonlinear-wave phenomena in one dimensional rotating shallow water. Part 2: high-resolution numerical simulations, J. Fluid Mech. 514, (2004), 35-63.
[7] F. Bouchut, Nonlinear stability of finite volume methods for hyperbolic conservation laws, and well-balanced schemes for sources, Frontiers in Mathematics series, Birkhäuser, (2004), ISBN 3-7643-6665-6.
[8] P. Deuflhard and F. Bornemann, Numerische Mathematik 2., Anfangs- und Randwertprobleme gewöhnlicher Differentialgleichungen, de Gruyter, (2002), ISBN 3-11-017181-3.
[9] T. Gallouët, J. Hérard and N. Seguin, Some approximate Godunov schemes to compute shallow-water equations with topography, Computers and Fluids, Vol. 32, (2003), 479-513.
[10] B. Gjevik, H. Moe and A. Ommundsen, Idealized model simulations of barotropic flow on the Catalan shelf, Continental Shelf Research Vol. 22, (2002), 173-198.
[11] L. Gosse, A.-Y. LeRoux. A well-balanced scheme designed for inhomogeneous scalar conservation laws, C.R. Acad. Sci. Paris Ser. I Math. 323, (1996), 543-546.
[12] L. Gosse, A well-balanced flux-vector splitting scheme designed for hyperbolic systems of conservation laws with source terms, Comp. Math. Appl. 39, (2000) 135-159 .
[13] S. Gottlieb, C.-W. Shu, E. Tadmor, Strong stability-preserving high-order time discretization methods, SIAM Rev., 43 (2001), pp. 89–112.
[14] J.M. Greenberg and A.Y. LeRoux. A well-balanced scheme for the numerical processing of source terms in hyperbolic equations, SIAM J. Num. Anal. 33 (1996), 1-16.
[15] R. Holdahl, H. Holden, and K.-A. Lie. Unconditionally stable splitting methods for the shallow water equations, BIT, Vol. 39, (1999) 451-472.
[16] G. Jiang and C.-W. Shu, Efficient implementation of weighted ENO schemes. J. Comp. Phys. Vol. 126, (1996) 202-228.
[17] S. Jin, A steady-state capturing method for hyperbolic systems with geometrical source terms, M2AN Math. Model. Numer. Anal. 35, (2001), 631-645.
[18] R.A. Klausen and N.H. Risebro, Stability of conservation laws with discontinuous coefficients, J. Diff. Eqn. 157, (1999), 41-60.
[19] C. Klingenberg and N.H. Risebro, Stability of a resonant system of conservation laws modeling polymer flow with gravitation, J. Diff. Eqn. 170, (2001), 344-380.
[20] A. Kurganov and D. Levy, Central-Upwind Schemes for the Saint-Venant System, M2AN Math. Model. Numer. Anal. 36, (2002), 397-425.
[21] R.J. LeVeque, Balancing source terms and flux gradients in high-resolution Godunov methods: the quasi-steady wave-propergation algorithm, J.Comp.Phys. 146, (1998) 346-356.
[22] N. Seguin, J. Vovelle, Analysis and approximation of a scalar conservation law with a flux function with discontinuous coefficient, M3AS 13, (2003), 221-257.

[23] J. Shi, C. Hu, and C.-W.Shu, A technique of treating negative weights in WENO schemes, J. Comp. Phys. 175, (2002), 108-127.
[24] C.-W. Shu, Total-variation-diminishing time discretization, SIAM J.Sci.Statist.Comp., 9. (1988), pp. 1073–1084.
[25] C.-W. Shu, Essentially non-oscillatory and weighted essentially non-oscillatory schemes for hyperbolic conservation laws, in Advanced Numerical Approximation of Nonlinear Hyperbolic Equations, edited by B. Cockburn, C. Johnson, C.W. Shu and e. Tadmor, Lecture Notes in Mathematics, Springer-Verlag, Berlin/New York, (1998), 325-432.
[26] C.-W. Shu and S. Osher, Efficient implementation of essentially non-oscillatory shock capturing schemes, J. Comp. Phys. Vol. 77, (1988), 439.
[27] R. J. Spiteri, S. J. Ruuth, A new class of optimal high-order strong-stability-preserving time discretization methods, SIAM J. Num. Anal. 40, No. 2, pp. 469–491.
[28] J.D. Towers. Convergence of a difference scheme for conservation laws with a discontinuous flux, SIAM J. Num. Anal. 38, (2000), 681-698.
[29] S. Vukovic and L. Sopta, ENO and WENO Schemes with the Exact Conservation Property for One-Dimensional Shallow Water Equations, J. Comp. Phys. Vol. 179, (2002) 593-621.
[30] Y. Xing C.-W. Shu, High Order Finite Difference WENO Schemes with the Exact Conservation Property for the Shallow Water Equations, Preprint (2004).

Appendix A. WENO Reconstruction

For completeness, we review the WENO reconstruction [16],[25] for uniform grids in 1D. Moreover, we wish to report the accuracy constants for the points in the Gaussian quadrature that we were not able to find elsewhere in the literature.

Given cell averages

$$u_i := \frac{1}{|C_i|}\int_{C_i} u(x)dx$$

on cell C_i and a fixed point $x^* \in C_j$, the WENO procedure provides a highly accurate piecewise polynomial approximation $R(x^*)$ of $u(x^*)$.

$$R(x^*) = u(x^*) + \mathcal{O}(\Delta x^{2r-1}) \tag{30}$$

1. Define r small stencils, composed of r cells, around the cell containing x_j

$$S_k := (x_{j+k-r+1}, x_{j+k-r+2}, ..., x_{j+k}), \qquad k = 0, ..., r-1$$

and one large stencil

$$\mathcal{T} := \bigcup_{k=0}^{r-1} S_k$$

which contains all the cells from the r smaller stencils.

2. Given cell averages u_j compute the interpolation polynomials $p_k(x)$ of degree $(r-1)$ associated with the stencils S_k for $k = 0, .., r-1$ and the higher order reconstruction polynomial $Q(x)$, of degree $(2r-1)$ associated with the large stencil $\mathcal{T}$. Here, interpolation is understood in the sense of cell averages.

3. Find the linear weights $C_0^r, ..., C_{r-1}^r$ such that:

$$Q(x^*) = \sum_{k=0}^{r-1} C_k^r p_k(x^*).$$

For the fifth order WENO reconstruction used in this paper we get the following weights:

(31)

x^*	C_0^3	C_1^3	C_2^3
$x_{j-\frac{1}{2}+}$	0.3	0.6	0.1
x_j	-0.1125	1.225	-0.1125
$x_{j+\frac{1}{2}-}$	0.1	0.6	0.3

For the 2D extension we need also weights for Gaussian points:

(32)

x^*	C_0^3	C_1^3	C_2^3
$x_j - \frac{\Delta x}{2\sqrt{3}}$	$\frac{70\sqrt{3}+1}{360\sqrt{3}}$	$11/18$	$\frac{70\sqrt{3}+1}{360\sqrt{3}}$
$x_j + \frac{\Delta x}{2\sqrt{3}}$	$\frac{70\sqrt{3}+1}{360\sqrt{3}}$	$11/18$	$\frac{70\sqrt{3}+1}{360\sqrt{3}}$

4. Compute the smoothness indicators

$$IS_k = \sum_{l=1}^{r-1} \int_{x_{j-\frac{1}{2}}}^{x_{j+\frac{1}{2}}} \Delta x^{2l-1} (p_k^{(l)})^2 dx,$$

where l denotes the l-th order derivative of p_k.

5. Compute the nonlinear weights based on the smoothness indicators

$$\omega_k := \frac{\alpha_k}{\alpha_0 + \cdots + \alpha_{r-1}}$$

where

$$\alpha_k := \frac{C_k^r}{(\varepsilon + IS_k)^2}, \quad k = 0, 1, ..., r-1.$$

Here ε is a real number which is introduced to prevent the denominator from becoming zero. To preserve accuracy, ε should satisfy the constraints

$$\begin{array}{ll} 0 < \varepsilon & \text{everywhere} \\ \varepsilon \ll IS_k & \text{in regions where the solution is smooth.} \end{array} \tag{33}$$

In the numerical experiments we use $\varepsilon = 10^{-6}$, except for the experiment in Section 3.2, where the IS_k are extremely small and we need to use $\varepsilon = 10^{-12}$.

6. The final WENO reconstruction is given by:

$$R(x^*) = \sum_{k=0}^{r-1} \omega_k p_k(x^*).$$

It is well known that the negative weights appearing in (31) may lead to oscillations at discontinuities [23]. Note however that this problem occurs only in the reconstruction of the point values at the locations $(x_i, y_{j\pm\alpha})$ and $(x_{i\pm\alpha}, y_j)$ which are needed only in the computation of $s_i^x(y)$ and $s_j^y(x)$, see (25) and (26). We have tested the following two approaches: first, we simply replaced the weights by the fourth order accurate choice of $C_0^3 := 0.25$, $C_1^3 := 0.5$ and $C_2^3 := 0.25$. Since these data midpoint appear only in the quadrature $S_{ci}^{(4)}$ for the source term, which is only fourth order accurate anyway, this does not decrease the overall order $(4, 5, 4)$ of the algorithm. The second cure is the splitting technique of Shi, Hu and Shu [23]. For the problems presented in this paper, this more expensive approach did not lead to superior results.

(Sebastian Noelle)
Institut für Geometrie und Praktische Mathematik,
RWTH Aachen, 52056 Aachen, Germany
E-mail address: `noelle@igpm.rwth-aachen.de`
URL: `http://www.igpm.rwth-aachen.de/~noelle/`

(Normann Pankratz)
Institut für Geometrie und Praktische Mathematik,
RWTH Aachen, 52056 Aachen, Germany
E-mail address: `pankratz@igpm.rwth-aachen.de`

(Gabriella Puppo)
Dipartimento di Matematica
Politecnico di Torino
Corso Duca degli Abruzzi 24
10129 Torino
E-mail address: `puppo@calvino.polito.it`

(Jostein Natvig)
SINTEF ICT, Forskningsveien 1, N0314 Oslo, Norway.
E-mail address: `Jostein.R.Natvig@sintef.no`